Internal state populations and velocity distributions of monatomic species ejected after the 1064 nm laser irradiation of barium

Maximiliano Rossa, Carlos A. Rinaldi, and Juan C. Ferrero[a)]
Centro Láser de Ciencias Moleculares, INFIQC and Departamento de Fisicoquímica, Facultad de Ciencias Químicas, Universidad Nacional de Córdoba, X5000IUS Córdoba, Argentina

(Received 12 December 2008; accepted 25 January 2009; published online 26 March 2009)

The plumes accompanying 1064 nm nanosecond pulsed laser ablation of barium in vacuum at three moderate incident laser fluences in the range of 5.3–10.8 J/cm^2 have been studied using both wavelength and time resolved optical emission spectroscopy and time-of-flight laser-induced fluorescence. Neutral atoms and both singly and doubly charged monatomic cations in excited states up to near the corresponding ionization limits are identified in the optical emission spectra. The population distributions of low-lying ($\leq$1.41 eV) "dark" states of Ba atoms measured by laser-induced fluorescence revel that the metastable ^3D_J and $^1D_2$ abundances in the plume are higher than predictions based on assuming a Boltzmann distribution. The ^3D_J and $^1D_2$ populations are seen, respectively, to decrease slightly and nearly no vary with raising fluence, which contrasts with the increasing trend that is observed in the ground-state Ba($^1S_0$) population. At all fluences, the time-of-flight distributions of the whole dark states and of various of the emitting levels are bimodal and well described by Maxwell–Boltzmann and shifted Maxwell–Boltzmann velocity functions, respectively, with different average translational temperatures $\langle T \rangle$ for each state. The $\langle T \rangle$ values for the dark states are insensitive to the fluence, while for all emitting species marked variations of $\langle T \rangle$ with fluence are found. These observations have been rationalized in terms of material ejection from the target being dominated by a phase explosion mechanism, which is the main contributor to the Ba($^1S_0$) population. Thermionic emission from the target surface can also release initial densities of free electrons and cations which, at the prevailing irradiances, will arguably interact with the incident laser radiation by inverse bremsstrahlung, leading to further excitation and ionization of the various plume species. Such a heating mechanism ensures that the energy injected to the plume will alter the propagation velocities of the primary inverse bremsstrahlung absorbers, i.e., cations, to a major extent than those of neutral atoms with increasing fluence. Electron-ion recombination occurring early in the plume expansion can lead to the generation of both neutral and ionic species in a manifold of long-lived Rydberg states, from which a radiative cascade will likely ensue. The distinct fluence dependences of the Ba(^3D_J) and Ba($^1D_2$) populations and velocity distributions show up the major complexity that distinguishes their populating mechanisms with respect to the remaining species. © *2009 American Institute of Physics*. [DOI: 10.1063/1.3089214]

I. INTRODUCTION

Studies on the pulsed laser ablation[1] (PLA) of solids have contributed substantially to the current knowledge of the interaction between intense electromagnetic fields and condensed matter.[2] Both available applications of PLA chiefly as a thin film deposition technique[3–5] and its use in the production of atomic,[6,7] molecular,[8] and cluster[5] beams for basic research, rely on these grounds. However, detailed understanding of PLA still imposes a considerable challenge that is conditioned by the variety of physical processes involved as well as the complex interrelation between the laser pulse parameters and both the nature and condition of the irradiated material. The case of bulk-metals ablated by nanosecond pulsed lasers is exemplary in this regard. In most cases, their primary ablation process can be described suitably within a thermal picture by which the laser light absorbed by the target degrades to lattice heat at subpicosecond time scales, causing metal atoms to be removed from the transiently heated bulk surface most likely as a result of evaporation or boiling.[1] Notwithstanding, a few previous studies on the PLA of gold at 248 (Refs. 9 and 10) and 532 nm (Ref. 11) and of alkaline-earth metals at 193 and 248 nm (Ref. 12) have suggested that electronic contributions[1] may also be involved at low laser fluences. Reported evidence in the case of alkaline-earth metals includes the observation of both ion desorption at a lower fluence than that predicted by the thermal vaporization model and a highly nonlinear relationship between the amount of desorbed ions and fluence.[12] On that basis, a photochemical mechanism was proposed in which the ultraviolet (UV) PLA of alkaline-earth metals at low irradiances is caused by MPI of the highest electron core of the atoms. This situation should be contrasted with the findings of a recent study of the 1064 nm PLA of alkaline-earth metals from this laboratory, where the total ablated monatomic mass of the various metals was measured at a range of incident laser fluences from the vaporization thresh-

[a)]Author to whom correspondence should be addressed. Electronic mail: jferrero@mail.fcq.unc.edu.ar. Tel: +54 351 4334169/80. FAX: +54 351 4334188.

old to the laser ablation regime.[13] Modeling of the data showed a correlation between the fluence above which laser ablation becomes dominant (the so-called critical fluence) and the Fermi energy of barium, which would suggest that the primary ablation process at 1064 nm is dominated by thermal contributions.

While thermal and electronic effects are basic to the PLA phenomenon, its nature can be concealed both as a result of collisions between particles in the plume and through plume-laser radiation interactions, which are very likely at the range of laser fluences (typically of $1-30$ J/cm^2 for most ablation laser wavelengths) used for thin film deposition.[1–5,14] This aspect is of utmost importance in PLA studies as the characterization of the resulting plumes is usually a major source of information about the underlying ablation process. To this aim, experimental data are frequently evaluated with respect to a number of predictions which are based on simple thermodynamic considerations. For example, the degrees of ionization immediately after cessation of the laser pulse within plumes ablated from metal targets are experimentally found to be >0.1, which are far higher than estimations based on assuming local thermal equilibrium at the target vaporization/boiling temperature in the gas plume.[3,4] Such a difference is usually ascribed to laser-induced multiphoton ionization (MPI) of the nascent plume that results in a rapid transition of the plume from an ionized gas to a plasma.[1–4,15–17] Related predictions of the internal state population distributions of neutral monatomic plume species would allow to anticipate an overwhelming majority of ground-state atoms given their typical ejection temperatures of the order of several thousand kelvin. This assumption, though, might require closer scrutiny in situations where low-lying metastable states are expected to be present in the ablation plume. The kinetic energy distributions of such metastable species may also differ substantially from those of the ground-state atoms, as exemplified by an earlier time-of-flight (TOF) laser-induced fluorescence (LIF) study of the 1064 nm PLA of barium at $\phi=5.3$ J/cm^2,[18] which in turn may have profound consequences on the quality of the deposited films of any suitable material. There are few reports of investigations of the electronic state populations of neutral atoms in plumes formed by PLA, involving only UV and visible (vis) laser wavelengths to compare with these thermal predictions.[19,20] The present work was undertaken mainly as an attempt to explore this topic in the case of the infrared (IR) PLA of a metal target, which is likely to favor thermally rather than electronically driven material ablation,[13,18] and at a range of laser fluences which are appropriate for plasma formation above the target surface in order to get information on the primary process under ablation conditions of practical use.

In this article, an improved characterization of the plume accompanying the PLA of barium at 1064 nm in vacuum is reported, using a combination of wavelength resolved optical emission spectroscopy (OES) and time resolved OES and LIF. These techniques allowed quantitative determinations of both the velocity distributions of various emitting and neutral dark monatomic species within the plume and the relative internal state population distribution of the latter, together with estimates of both the composition and the extent of the ionization and electronic excitation of the ablated material, at laser fluences in the range of $\phi=5.3-10.8$ J/cm^2. Preliminary results of the population distributions of dark Ba atoms at $\phi=7.6$ J/cm^2 have been reported previously as a part of a recent study of the Ba(^3P)+N_2O reaction dynamics at hyperthermal collision energies.[7] Taken altogether, the results provide not only a comprehensive picture of the plume dynamics following IR PLA of barium but also clues to the primary ablation mechanism. In addition, they show up the major complexity that distinguishes the mechanisms populating the lowest-lying excited states of neutral Ba.

II. EXPERIMENT

The ablation apparatus comprises a high-vacuum stainless steel chamber equipped with several side arms, sealed by either a quartz or a BK7 glass window, permitting optical contact with the target. Chamber evacuation is by means of a diffusion pump (Edwards *Diffstak* 250/2000 M, 2000 l/s), backed by a two-stage rotary pump (Edwards E2 M40, 50 m^3/h), which together maintain the chamber at a base pressure $<1\times10^{-6}$ Torr. The 1064 nm output of a Q-switched neodymium:yttrium aluminum garnet (Nd:YAG) laser [Laseroptics LND 532, 10 ns full width at half maximum (FWHM) pulse duration, 5 Hz repetition rate] was steered through one of the side arms using a prism and a set of mirrors and focused onto the target surface at normal incidence using a biconvex lens (BK7, 40 cm focal length) placed before the entrance BK7 glass window. The target consisted of a 22 mm in diameter $\times\sim2$ mm thick disk of barium (Alfa Aesar, purity $>99\%$), mechanically polished on the face to be exposed to the incident laser beam. The target was mounted on a homebuilt rotation/two-dimensional translation stage and rotated during the experiments by a stepper motor so as to allow ablation of a fresh area of the target surface with each laser shot. Because of target erosion, though, lateral translation of the target was periodically required in order to minimize groove formation. The circular ablation laser footprint at the focal point was estimated to be 0.25 mm in diameter by digital image analysis of a scan of the burned pattern on a photosensitive paper placed at the target position. The ablation laser output energies were controlled in order to set the incident laser fluence ϕ to the three specific values of 5.3, 7.6, and 10.8 J/cm^2. To determine the actual laser energies that reached the target, the vacuum chamber was vented before experiments and the unfocused incident laser energies were measured by placing a Scientech 756 calorimeter head inside the vacuum chamber; the transmission loss through the focusing lens was determined separately and periodically checked.

In order to sample the neutral/ionic particle flux propagating along the normal to the target surface, the central portion of the resulting ablation plume was selected with a collimating device, consisting in a sheet with a 0.2 cm in diameter sampling orifice, which was positioned 0.3 and 1.25 cm from the ablation volume for OES and LIF measurements, respectively.

Optical emission accompanying the ablation plume was

viewed at 90° to the central axis of the ablation plume and at a fixed distance d between the barium disk and the center of the observation region of 3.3 cm. Emission light was collected by a biconvex lens (BK7, 5 cm focal length) and focused onto the entrance slit of a 0.30 m monochromator (McPherson 218, 1200 lines/mm grating, wavelength range: 105–1000 nm), equipped with a fast photomultiplier tube (PMT) (Hamamatsu R636, 2.0 ns rise time) with spectral response in the range of 185–930 nm. The sensitive spectral range of the combined detection system is between 350 and 930 nm. The collecting lens was positioned 6.6 cm from the plume central axis and 20.6 cm from the entrance slit of the monochromator. The acceptance cone of this sharply focused arrangement determined the volume of the plasma from which emission was collected, which was (80.5 ± 0.5) mm^3. Emission spectra were obtained by scanning the monochromator with the entrance and exit slit widths set to 150 μm and passing the PMT output via a transient digitizer (Thurlby DSA 524) to a personal computer for data processing and storage. Signals from four laser shots were averaged and time integrated for each spectral point; under these conditions, the spectral resolution was 0.5 nm. Alternatively, TOF transients of the relevant emitting species into the volume viewed by the optics detection system were obtained by tuning the grating to the center wavelength of the appropriate emission line and using wider slit widths. The $6s6p\ ^1P_1$, $^3P_1$ states of Ba atoms were monitored by their emission lines at 553.55 and 791.13 nm, respectively, while the emission lines at 455.40 and 709.55 nm were employed to detect the $^2P_{3/2}$ and the $5s^25p^54f[3/2]_2$ states of Ba^+ and Ba^{2+} ions, respectively.[21,22] The PMT output was then passed through a fast preamplifier (Stanford Research Systems SR455) to a digital oscilloscope (Tektronix TDS 3034B) for data acquisition and storage. An average of 512 shots was used to generate the time profiles.

The $6s^2\ ^1S_0$, $6s5d\ ^1D_2$, and $6s5d\ ^3D_{1,2,3}$ dark states of Ba atoms were probed by suitable two-level LIF schemes.[18,23] A pulsed dye laser (Lumonics HD500, 0.04 cm^{-1} FWHM bandwidth) was used to excite the atomic fluorescence, operating on Rhodamine 575 (for Ba ground-state measurements) and dicyanomethylene (for Ba metastable state measurements) dyes (Exciton) and pumped by a Q-switched Nd:YAG laser (Spectra-Physics INDI 40–10, 10 ns FWHM pulse duration, 5 Hz repetition rate) at 532 nm. The dye laser beam was loosely focused to ~2 mm diameter into the center of the ablation plume by a planoconvex lens (BK7, 40 cm focal length). Two 10 cm long blackened baffles were placed in the entrance and exit side arms to minimize the background from scattered laser light. In the current experimental geometry, the probe laser beam propagated perpendicularly to the axis of the optical system for the fluorescence collection and at 45° to the central axis of the ablation plume. The dye laser was operated with output energies in the range of 7.0–20.0 μJ/pulse, as measured by a pyroelectric detector (Laser Precision Corporation RJP735), but the energies that reached the excitation volume were only 11% of these owing to loses in the optical system. Further reduction in the dye laser energy by a factor of 10^{-4} with a variable attenuator prior to focusing was required to avoid optical pumping effects and to maintain the linearity of the LIF signals on the dye laser power. The atomic fluorescence was imaged through a telescope onto the same scanning monochromator and PMT combination above mentioned, and the PMT output was then amplified and digitalized for data acquisition and processing. The waist of the probe laser beam and the solid angle of the optical system collecting the fluorescence determined the excitation volume from which the LIF signal was recorded, which was approximately cylindrical and 2 mm in diameter $\times 1.5$ mm length. Relevant atomic barium TOF data were collected by tuning the dye laser to individual Ba spectral lines and recording the LIF signal as a function of the ablation-probe delay Δt at a fixed distance l between the barium disk and the excitation laser of 3.3 cm. An average of 128 shots was used to generate each data point of the time profiles. For the determination of the population ratios of the different dark species, the corresponding LIF-TOF profiles were numerically integrated and further processed as described in Sec. III C.

Wavelength calibration was verified using Ba atomic lines and lines from low pressure H and Ne lamps. A master pulse/delay generator (Berkeley Nucleonics Corporation 500 C) was used to control the timing sequence of the experiments.

Although the distribution of Ba_n species in the beam has not been directly measured in this laboratory, the amount of small polyatomic species is considered to be negligible since we detected neither emission nor LIF other than those of monatomic Ba species (see Sec. III A).

III. RESULTS AND DISCUSSION

A. Optical emission spectra

Before addressing to the spectral details of the plumes accompanying 1064 nm PLA of barium in vacuum, it is instructive to make some remarks on the broad features of such plumes when side viewed to the bare eye. An intense white emission was clearly visible close to the laser focus onto the target surface, in addition to a more extensive, jetlike pink glow, distributed symmetrically about the surface normal. While the white emission observed here can be associated to bremsstrahlung,[14] the visible glow could be indicative of the presence of a significant amount of electronically excited neutrals and cations.[3,4,24,25] This latter emission was monitored using time integrated, wavelength-dispersed OES in order to analyze the composition and the extent of ionization and electronic excitation of the ablated material.

The spectral shapes of the Ba plume emissions recorded at $d=3.3$ cm were quite similar for the three fluences used in this work. Figure 1 shows a representative high resolution ($\Delta\lambda=0.5$ nm) spectrum over the range of 400–800 nm obtained at $\phi=7.6$ J/cm^2. This is dominated by the Ba atom resonance $6s6p\ ^1P_1 \rightarrow 6s^2\ ^1S_0$ line at 553.55 nm and, in fact, analysis showed that electronically excited neutral Ba atoms and both singly and doubly charged Ba ions (henceforth referred as to Ba^*, Ba^{+*}, and Ba^{2+*}, respectively) are responsible[21,22] for all of the emissions observed. It should be noted that the relative intensities of the various features in the emission spectra were observed to vary with both d and

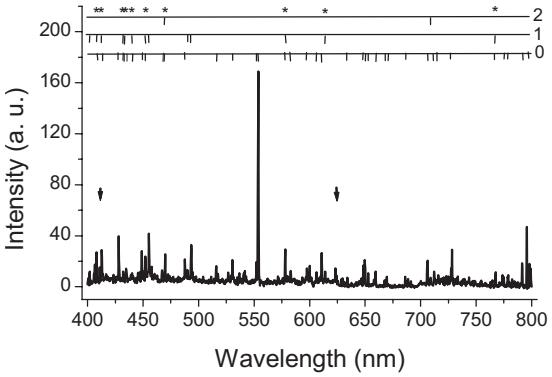

FIG. 1. Time integrated spectrum of the Ba plume emission recorded at a viewing distance of 3.3 cm from the focal spot along the Ba surface normal and at $\phi=7.6$ J/cm^2. The spectrum has been corrected by spectral response of the detection system (Ref. 7). Ba^{z+*} emission lines are indicated by the combs above the spectrum (arranged by z, as labeled on the right), while the stars above the combs indicate a number of lines that are not discernable within the spectral resolution. "↓" indicates lines appearing in second order, i.e., those at 411.03 and 623.34 nm associated with, respectively, the Ba^{+*} ($9d\ ^2D \rightarrow 6p\ ^2P^o$) multiplet at ~205.3 nm and the $5s^25p^54f[9/2]_4 \rightarrow 5s^25p^55d[7/2]_8$ transition of Ba^{2+*} at 311.92 nm.

ϕ so that (i) the Ba^{+*} and Ba^{2+*} emission line intensities were greater than those associated with neutral Ba^* atoms at small viewing distances (i.e., at $d<1$ cm); (ii) the ionic emissions decayed faster than the neutral lines with increasing d; and (iii) for a given d, all emission line intensities increased with ϕ, in an extension dependent on the nature of the emitting species so that the ratio of the Ba^{+*}/Ba^* emission intensities grew at higher ϕ while the Ba^{2+*}/Ba^* ratios remained nearly the same. Also worth mentioning is that many of the emissions originate from highly excited Rydberg states of Ba neutrals and cations, e.g., the 469.91,[26] 402.41, and 709.55 nm emissions attributable to the $6s9d\ ^1D_2$, $10d\ ^2D_{3/2}$, and $5s^25p^54f[3/2]_2$ states of Ba^*, Ba^{+*}, and Ba^{2+*}, respectively, which lie correspondingly at 4.88, 14.27, and 36.11 eV above the ground state of neutral barium. In the former two cases, the energies are certainly close to the values of 5.21 and 15.21 eV for the ionization energies for forming the Ba^+ and Ba^{2+} ions from the ground-state neutral atom, respectively.

Such findings are in good accord with those of previous OES studies of UV/IR PLA of a number of elemental targets in vacuum.[24,25,27,28] Taken altogether, these results indicate that the fraction of the Ba plume which is present in electronically excited states is predominantly monatomic in composition, and show up remarkable levels of ionization and excitation of such plume constituents.

Two additional observations can provide clues to the formation routes of the emitting species. The first one is that all of the more intense emission lines of Ba^* and Ba^{+*} expected[21] in the range of 400–800 nm were observed, indicating a lack of specificity in the production of the excited states. A similar behavior was previously reported in the case of 193 nm PLA of graphite.[25] The second one is the observation of emissions at time scales (several micro seconds) larger than the corresponding radiative lifetimes [e.g., 8.37 ns (Ref. 29) for the $6s6p\ ^1P_1$ excited state of Ba]. This is in accord with previous findings for PLA of graphite, Cu, Al, and Si at 193 nm,[24,25] and Ti at 248 nm,[30] and support the view that most of the Ba, Ba^+, and Ba^{2+} emitting levels present at larger d are populated post pulse by collisional and/or radiative cascade from a manifold of long-lived Rydberg states, which are initially formed via collisionally assisted electron-ion recombination (EIR). Such arguments were previously used to rationalize the similarity between the TOF distributions of Ba and Ba^+ emitting states arising from 1064 nm PLA of barium at $\phi=5.3$ J/cm^2.[18] They can also account for the apparent nonspecific excited state production process in the present time integrated wavelength-dispersed OES measurements: Collisional and/or radiative cascade will populate a wide range of comparatively low-lying emitting levels. This is likely to result in a highly non-Boltzmann, nonspecific excited state population distribution from which a rich plume emission spectrum, like that shown in Fig. 1, could plausibly arise.

The above interpretation implies that the observation of any Ba^{z+*} emissions is an indicator of the existence of $Ba^{(z+1)+}$ ions in the plume prior to EIR; thus, the mechanism by which such multiply charged ions might be initially formed merits further assessment. Before addressing to this issue, we first consider OES- and LIF-TOF measurements of the velocity distributions of several Ba, Ba^+, and Ba^{2+} species as a function of the ablation laser fluence. Overall, the data can be informative not only on the primary ablation mechanism but also on possible ionization processes occurring in the early stages of the ablation plume.

B. Velocity distributions of neutral and ionic monatomic species

Figure 2 shows the OES-TOF distributions of the relevant emitting states of Ba, Ba^+, and Ba^{2+}, which were measured at $\phi=5.3$ J/cm^2 for Ba^{2+} and at $\phi=7.6$ and 10.8 J/cm^2 for the three species. All of the atomic/ionic species TOF spectra show an initial fast spike at which $t<1$ μs can be attributed to emissions associated to the intense white plasma observed near the Ba target and thus taken as indication of the zero time of the experiments. All of these distributions are clearly bimodal. In the case of $Ba(^3P_1)$ at 10.8 J/cm^2, the slow component is shifted to earlier arrival times in comparison with the TOF profile at 5.3 J/cm^2, where $Ba(^3P_1)$ showed two clearly resolved components;[18] this makes the slow component to appear immersed in the decay part of the fast, larger components (Fig. 2). This is more evident in the TOF spectra of $Ba(^1P_1)$, and to a lesser extent in those of the ionic species as ϕ is increased from 7.6 to 10.8 J/cm^2.

Figure 3 shows the number density LIF-TOF distributions $N(\Delta t)$ of the relevant dark states of Ba atoms measured at $\phi=7.6$ and 10.8 J/cm^2. Comparison with the previously reported data at 5.3 J/cm^2 (Ref. 18) shows that the shape and peak of the TOF distributions for all of the dark states probed are hardly altered by a twofold increase in ϕ in the range of 5.3–10.8 J/cm^2.

It should be mentioned that the different observation volumes used in the present OES and LIF experiments do not seriously affect the velocity distributions that are derived

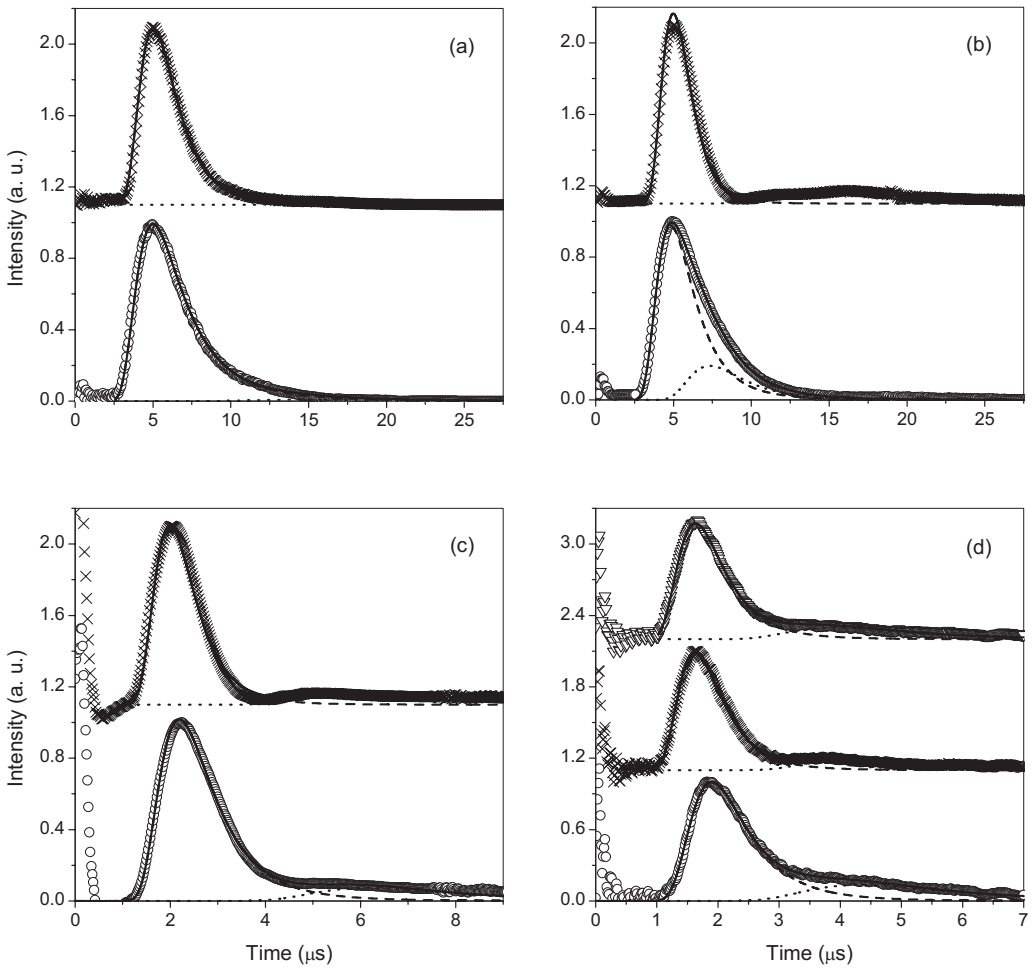

FIG. 2. OES-TOF distributions measured at ϕ=5.3 (▽), 7.6 (×), and 10.8 (○) J/cm^2 for (a) the neutral Ba atoms in the $^3P_1$ state; (b) the neutral Ba atoms in the $^1P_1$ state; (c) the singly charged Ba^+ ions in the $^2P_{3/2}$ state; and (d) the doubly charged Ba^{2+} ions in the $5s^25p^54f[3/2]_2$ state. Also shown are total fits (—) of the data to a superposition of two shifted MB functions: (---) fast component; (···) slow component.

from the TOF profiles of all of the dark and emitting species probed here because collimation of the ablation plume significantly reduces the slow radial components in both cases.[18]

Most general features characterizing the propagation velocities of the various Ba^{z+} species along the plume axis can be unveiled by comparing their peak velocities, computed as the ratio of the relevant flight distance to the corresponding peak TOFs. These are shown as a function of ϕ in Fig. 4, which includes the corresponding peak velocities at ϕ =5.3 J/cm^2 that are derived from data reported previously.[18] The peak TOFs of the dark species were taken from their TOF profiles previously converted from number density to flux distributions $N'(\Delta t)$ employing a correction factor of $l/\Delta t$ to account for the fact that atoms with lower velocities are preferentially detected by LIF. Despite the limited number of data points, it is readily apparent that the derived peak velocities are rather insensitive to the incident laser fluence. However, they consistently show a positive correlation with charge state and electronic excitation for neutral Ba, within the fluence range used in this work. Similar trends were found for the ϕ-dependence of the various Ba^{z+} mean velocities, calculated from the whole velocity distributions that derive from the corresponding TOF profiles. Indeed, the various Ba^{z+*} propagation velocities show an scaling with the charge of the ionic $Ba^{(z+1)+}$ precursors: For example, the peak velocities derived from Ba^{+*} emissions are roughly twice those from Ba^* emitters (taken respectively as signifiers of Ba^{2+} and Ba^+ ions). Such observations, particularly the charge-state dependence of propagation velocities are in good accord with previous PLA studies of, for example, Cu, Al, Si, graphite,[24] Nd,[20] and Sn (Ref. 31) targets. The present findings are also in line with those of Ref. 24 in that the monatomic dark neutral species present in the ablation plume have lower propagation velocities than higher-lying emitting state neutral atoms, although the use of the LIF technique allowed here to discriminate between ground and metastable state dark neutral Ba atoms.

The insensitivity of the various Ba^{z+} peak/mean velocities to ϕ is in agreement with the observation in an earlier PLA study on gold at 1064 nm by TOF quadrupole mass spectrometry[32] (QMS) that the mean velocities of Au^+ and Au^{2+} ions remained constant over a substantial range of ϕ. Production of faster moving Au^{z+} ions in higher charge states ($z \leq 10$) was observed at the highest fluences. Also, two recent PLA investigations on tin at 1064 nm by OES (Ref. 31) and on nickel at 532 nm by TOF-QMS (Ref. 33) consistently reveal that increasing ϕ results in a decrease in the propaga-

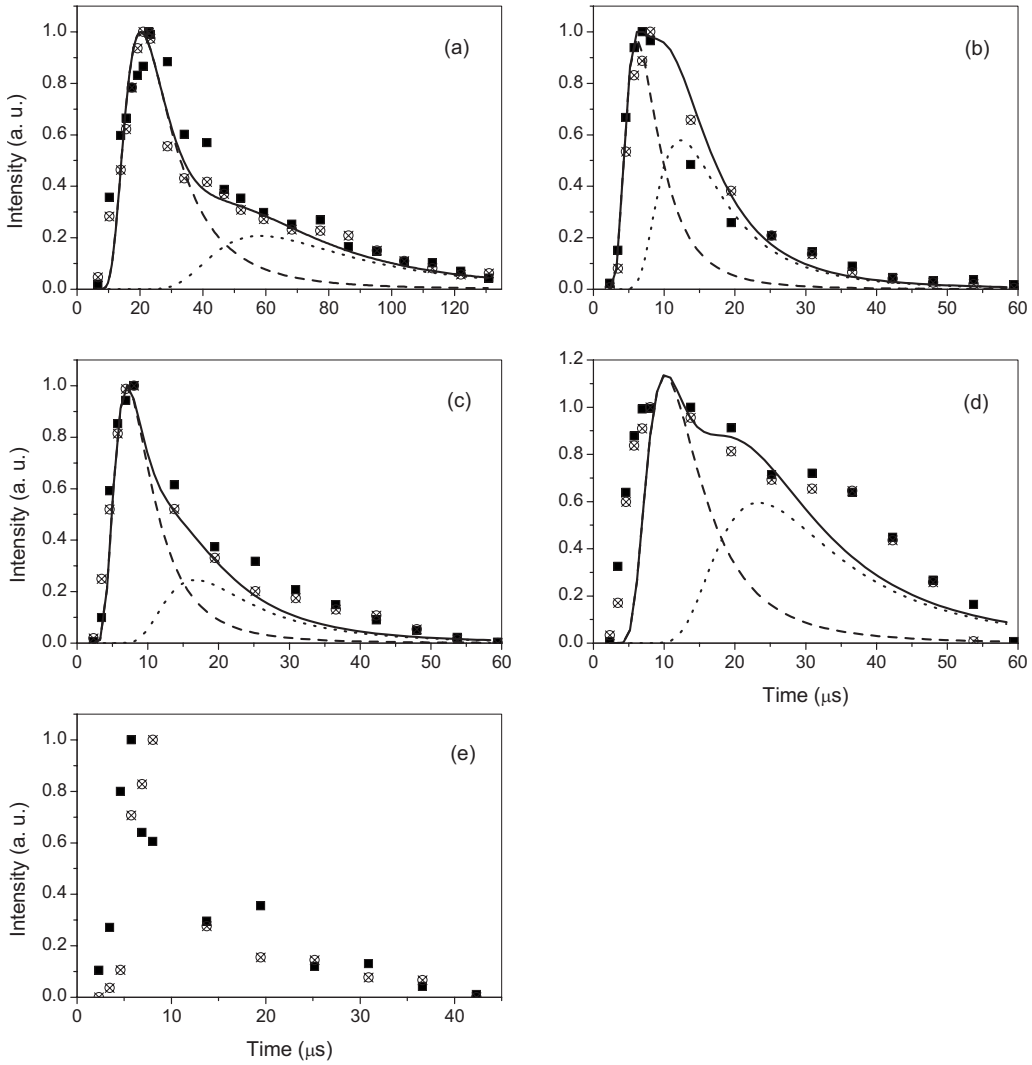

FIG. 3. Number density LIF-TOF distributions measured at ϕ=7.6 (■) and 10.8 (⊗) J/cm^2 for Ba atoms populating the (a) $^1S_0$, (b) $^3D_1$, (c) $^3D_2$, (d) $^3D_3$, and (e) $^1D_2$ states. Also shown are total fits (—) of the data at 10.8 J/cm^2 to a superposition of two shifted MB functions: (---) fast component; (···) slow component.

tion velocities associated to the Sn^{+*} and Ni^{2+} ions, respectively. In addition, no change was observed for the Ni^{3+} ions. Such behaviors were explained assuming that increasing ϕ leads to the production of higher charged ions to the expense of the translational energy of the remaining, low charged species. A similar plume dynamics is arguably operative in the 1064 nm PLA of barium: Corroboration of such proposal would require an observation of $Ba^{z+}(z>2)$ ions in the plume, which in turn would reinforce the above suggestion on the existence of $Ba^{(z+1)+}$ ions prior to EIR. Unfortunately, this was not feasible in the present experiments since all of the documented[34] transitions for such ionic species, involving only Ba^{3+} and Ba^{4+}, lie in the wavelength region lower than 100 nm, which is out of the sensitive spectral range of the detection system used.

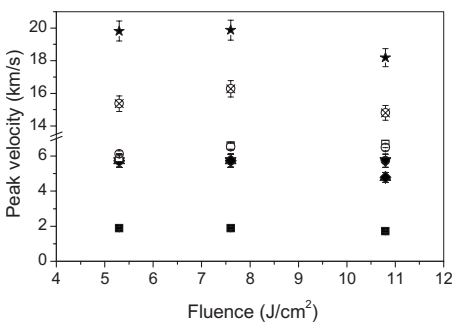

FIG. 4. Measured ablation laser fluence dependences of the peak velocities for the neutral Ba atoms in the $^1S_0$ (■), $^3D_1$ (●), $^3D_2$ (▲), $^3D_3$ (▼), $^1D_2$ (♦), $^3P_1$ (□), and $^1P_1$ (○) states; the singly charged Ba^+ ions in the $^2P_{3/2}$ (⊗) state; and the doubly charged Ba^{2+} ions in the $5s^25p^54f[3/2]_2$ (★) state. Data at ϕ=5.3 J/cm^2 were taken from previous work (Ref. 18).

For a more complete analysis, the various Ba^{z+} TOF distributions were fitted to different model functions assumed for the corresponding velocity distributions. Thus, the data for the emitting states required the addition of two terms of the flux-weighted shifted Maxwell–Boltzmann (MB) function,

$$I(v) \propto v^3 \exp[-m(v-v_0)^2/2kT], \quad (1)$$

where v denotes the velocity, v_0 is the flow velocity parallel to the surface normal, m is the Ba atomic mass, T is the translational temperature, and k is the Boltzmann constant.

TABLE I. Parameters that characterize both the two components and the whole of the velocity distributions of each Ba atomic and Ba^+ ionic species.

	Fluence (J/cm^2)							
	7.6				10.8			
Component	v_0 (km/s)	T (10^3 K)	Relative contribution (%)	$\langle T\rangle$ (10^3 K)	v_0 (km/s)	T (10^3 K)	Relative contribution (%)	$\langle T\rangle$ (10^3 K)
$Ba(^1S_0)$ Slow	⋯	1.5 ± 0.3	24	6.4 ± 0.5	⋯	1.3 ± 0.6	34	7.7 ± 0.6
Fast	⋯	7.9 ± 0.4	76		⋯	11 ± 2	66	
$Ba(^3D_1)$ Slow	⋯	18.6 ± 0.2	32	71 ± 4	⋯	30 ± 6	54	71 ± 3
Fast	⋯	95 ± 4	68		⋯	120 ± 7	46	
$Ba(^3D_2)$ Slow	⋯	16.2 ± 0.8	38	58 ± 2	⋯	16.2 ± 0.3	36	64 ± 2
Fast	⋯	85 ± 2	62		⋯	90 ± 6	64	
$Ba(^3D_3)$ Slow	⋯	8.3 ± 0.4	52	25 ± 3	⋯	8.3 ± 0.4	52	25 ± 3
Fast	⋯	44 ± 4	48		⋯	44 ± 4	48	
$Ba(^3P_1)$ Slow	1.7 ± 0.1	2.1 ± 0.4	2	48 ± 9	1.6 ± 0.9	5.5 ± 0.2	2	89 ± 3
Fast	4.8 ± 0.1	48.7 ± 0.3	98		3.3 ± 0.8	90.9 ± 0.2	98	
$Ba(^1P_1)$ Slow	1.1 ± 0.1	9.4 ± 0.1	23	24 ± 4	3.3 ± 0.1	22.3 ± 0.1	22	51 ± 4
Fast	5.6 ± 0.3	27.8 ± 0.1	77		4.8 ± 0.7	59.5 ± 0.1	78	
$Ba^+(^2P_{3/2})$ Slow	4 ± 2	31 ± 1	14	231 ± 6	3 ± 1	32 ± 6	13	310 ± 60
Fast	12 ± 2	263 ± 1	86		8 ± 1	349 ± 7	87	

Tables I and II show the parameters obtained from the best fits, together with a weighted average temperature $\langle T\rangle$ for the whole velocity distribution of each emitting species. In contrast, all of the $N(\Delta t)$ LIF-TOF profiles could be fitted to a superposition of two terms of the number density MB function,

$$N(v) \propto v^2 \exp[-mv^2/2kT]. \quad (2)$$

Values of T derived from the best fits, and of $\langle T\rangle$ calculated for the whole velocity distributions of each dark species are listed in Table I. As in the previous PLA studies of barium,[18] the low number of data points in the low-velocity region prevented an accurate fit for the $^1D_2$ state; from the resemblance between the general forms of the $^1D_2$ and ^3D_J TOF distributions, though the $^1D_2$ velocity distributions could also be expected to be well described by a MB function with a set of parameters similar to those of the remaining metastables.

TABLE II. Parameters that characterize both the two components and the whole of the velocity distributions of the Ba^{2+} ionic species in the $5s^25p^54f[3/2]_2$ state.

Fluence (J/cm^2)	Parameter	Component	
		Slow	Fast
5.3	v_0 (km/s)	5 ± 2	13 ± 1
	T (10^3 K)	97 ± 1	473 ± 9
	Relative contribution (%)	19	81
	$\langle T\rangle$ (10^4 K)	40 ± 1	
7.6	v_0 (km/s)	7 ± 2	14 ± 1
	T (10^3 K)	42 ± 6	417 ± 9
	Relative contribution (%)	14	86
	$\langle T\rangle$ (10^4 K)	36 ± 6	
10.8	v_0 (km/s)	4 ± 1	10 ± 2
	T (10^3 K)	97 ± 3	403 ± 1
	Relative contribution (%)	23	77
	$\langle T\rangle$ (10^4 K)	33 ± 1	

Comparison of the weighted average temperature for the $Ba(^1S_0)$ and $Ba(^3D_J)$ whole velocity distributions on one hand shows that the latter (and arguably those for $^1D_2$ also) are much broader, a feature[18] that was already observed at $\phi=5.3$ J/cm^2. Also in common with previous observations, the metastable slow velocity components are found here to be centered at velocities near those for the fast, major components of the ground state (as evidenced by the corresponding T values). On the other hand, at the prevailing fluences both components for $Ba^{2+}(5s^25p^54f[3/2]_2)$ are broader and centered at higher velocities than those of $Ba^+(^2P_{3/2})$, and similar considerations hold when comparing the latter with the emitting neutral Ba velocity distributions (cf. Tables I and II). The different MB functions required to fit the emitting and dark-state TOF distributions prevent a straightforward comparison between the T and $\langle T\rangle$ absolute values that derive from both cases. Nevertheless, such an approximation is certainly significant when mainly intended to quantify the evolution with ϕ of the total width of the velocity distributions along the observation axis for these different plume species. Thus, Fig. 5 illustrates the ϕ dependence of the $\langle T\rangle$ values for the various velocity distributions; data[18] determined previously at 5.3 J/cm^2 are also included in the plot. Three different trends in the variation of the Ba^{z+} whole velocity distributions with incident laser fluence are observed: (1) for all of the Ba dark states no discernible ϕ-dependence is observed; (2) values of $\langle T\rangle$ for both Ba emitting states and for $Ba^+(^2P_{3/2})$ display two time to four time increases when ϕ is increased from 5.3 to 10.8 J/cm^2; and (3) the $\langle T\rangle$ values for $Ba^{2+}(5s^25p^54f[3/2]_2)$ slightly decrease with increasing ϕ. This highlights some differences between the various parameters characterizing the propagation velocities of all plume constituents that have been extracted from their TOF profiles. Most notably, the ϕ-dependence of the $\langle T\rangle$ values for all of the emitting species suggests a far more marked

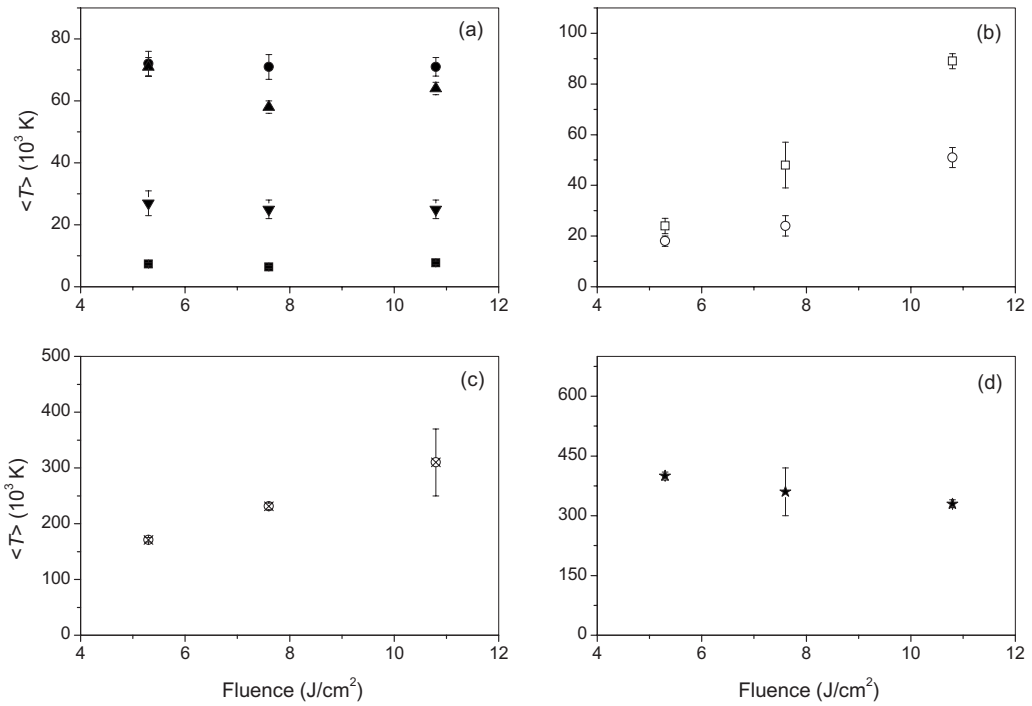

FIG. 5. Measured ablation laser fluence dependences of the weighted average temperatures for: (a) the neutral Ba atoms in the $^1S_0$ (■), $^3D_1$ (●), $^3D_2$ (△), $^3D_3$ (▼) states; (b) the neutral Ba atoms in the $^3P_1$ (□) and $^1P_1$ (○) states; (c) the singly charged Ba^+ ions in the $^2P_{3/2}$ (⊗) state; and (d) the doubly charged Ba^{2+} ions in the $5s^25p^54f[3/2]_2$ (★) state. Data at ϕ=5.3 J/cm^2 in (a)–(c) were taken from previous work (Ref. 18).

variation in the translational energy content than indicated by the corresponding peak/mean velocities. It seems that for the present PLA system and conditions the translational temperatures are more sensitive to the propagation properties of all of the plume constituents than either their peak or mean velocities.

These results can be rationalized by recognizing that thermal contributions to the primary ablation process are likely to dominate the ns 1064 nm PLA of barium at the moderate laser irradiances (~0.5–1 GW/cm^2) of the present experiments. As pointed out in Sec. I, recent modeling of the data of ablated monatomic total Ba mass as a function of incident laser fluence provides further support for this suggestion.[13] As before,[18] explosive boiling appears the most probable photothermal mechanism at the prevailing laser irradiances: Within this picture, the IR high-power, 10 ns long ablation laser pulse used here induces a rapid heating of a highly localized surface layer of the Ba target, bringing it near to its critical point and ultimately leading to its breakdown into a mixture of vapor and liquid droplets that are ejected from the target. Free electrons along with cations will likely be present in the plume through thermionic emission from the hottest region of the target surface (possibly supplemented by a number of gas phase ionization processes; see below) and those ions will be accelerated out of the focal volume by the so-called dipolar diffusion mechanism, as a result of Coulombic fields generated by the fastest moving electrons that escape from the expanding plume at early times.[35] This can account for the apparent scaling of the various Ba^{z+*} peak velocities with ionic charge: Coulombic fields scale with the charge of any given ionic $Ba^{(z+1)+}$ precursor so that correlation can be expected to appear in the terminal propagation velocities of the respective Ba^{z+*} species produced by EIR. This model also makes allowance for the presence in the plume of neutral Ba atoms, e.g., those populating low-lying dark states, with lower peak velocities than the neutral Ba^* species. In contrast to the latter that would result mainly from gas phase EIR, a major fraction of the former would have been ejected from the target surface as neutrals and thus not subject to Coulombic acceleration at all. The significant broadening of the Ba($^1S_0$), Ba(^3D_J), and Ba($^1D_2$) whole velocity distributions would thus result from the large temperature changes accompanying the phase explosion heating trajectory. In addition, a minor fraction of ^3D_J and $^1D_2$ states could arguably originate from radiative decay of higher-lying excited states, giving rise to the increased broadening of their total velocity distributions in comparison to those of $^1S_0$.

The presence of large particulates in the ablation plume can be inferred from the current LIF-TOF experiments, where it was found at all fluences that occasional bright spots originating from the probe laser excitation volume were clearly visible to the bare eye at ablation-probe delays (t =160–230 μs) large enough so that all dark-state Ba LIF signals have vanished. The temporal and spatial (owing to plume collimation) localization of this phenomenon assures that it is associated with the laser ablation process. Observation of such spots even at different probe laser wavelengths, where Ba atomic/ionic LIF transitions are not expected, suggests that they originate in elastic light scattering by delayed large particulates that are present in the plume. As above, the propagation velocities of such particulates along the plume axis could be estimated by the ratio of the relevant flight distance to the corresponding TOFs to be in the range of

140–210 m/s. Similar values have been reported previously for the propagation velocities of macroparticles ejected from various target materials and using very different laser wavelengths.[36–38] Consistent with other recent studies,[39] it is suggested here that explosive boiling is the most plausible formation mechanism for such apparently delayed macroparticles following nanosecond laser irradiation of barium.

Substantial interactions of the nascent plume with the ablation laser radiation can also be anticipated[18] at the present range of incident laser fluences, which is within the saturation region of the ablated monatomic Ba mass (see Fig. 5 of Ref. 13). This saturation behavior is generally ascribed to the target being screened off from the later part of the laser pulse as a result of significant absorption by the plume.[16,40,41] In particular, the inverse bremsstrahlung (IB) effect will be very efficient here because of the large absorption coefficient that characterize free electrons at the IR excitation wavelengths used.[14] A portion of the absorbed energy will be redistributed into the ensemble of plume constituents by collisions or Coulombic forces, thereby leading to an increase in both translational and electronic energies as well as to further ionization of the various species formed during the laser pulse. This, in turn, will result in a rapid transition of the plume from an ionized gas to a plasma (matching our observation of a plasma above the Ba target). Indeed, the high levels of plume excitation and ionization revealed by the present OES measurements, as well as the finding of high translational temperatures for the neutral and ionic Ba species are fully consistent with this heating mechanism.

Consideration of possible mechanisms for the initial formation of multiply charged $Ba^{(z+1)+}$ ions can now be resumed. On the basis of the evidence presented here and elsewhere,[13,18] it is apparent that direct ejection of ions from the target surface as a result of a photochemical mechanism[12] should be dismissed, which leads to thermionic emission as the most plausible surface mechanism for the generation of initial free electrons and positive ions in the ablation plume. Such species will further act as very efficient initial absorbers of the IR laser pulse via electron-ion (e-i) IB.[17,41,42] A number of gas phase ionization processes may also contribute, among which nonresonant MPI is often invoked as the most probable.[1,3,4] Nevertheless, closer scrutiny suggests that it should be disregarded here: Given that the photon energy of a 1064 nm laser pulse is 1.17 eV, formation of Ba^+ and Ba^{2+} from Ba atoms in the ground state by MPI would require the absorption of five and thirteen of such photons, respectively, which is improbable at the prevailing laser irradiances (≤ 1 GW/cm^2). Instead, ionization from highly excited states can become important in the later part of the pulse as a result of the generation of such species in the plasma via EIR.

The observation of two clearly resolved TOF components for the emitting Ba^{z+*} species is in accord with an acceleration of the ionic $Ba^{(z+1)+}$ precursors by a two-electron-temperature mechanism, as a result of preferential energy input to the leading part of the expanding plume via IB. This could generate an escaping tail of energetic electrons in advance of the remaining, cold electron distribution, which together might act as two sequential Coulombic accelerators leading to two-peak structures[40] in the Ba^{z+*} TOF distributions. Such effects could also result in a ϕ-dependent evolution of these TOF distributions from double to single peaked within a relatively narrow laser fluence range, as observed here and previously shown by Bulgakova *et al.*[40] for the total ion TOF profiles that derive from the 1064 nm PLA of graphite.

An assessment of the laser fluence dependence of the various dark and emitting species velocity distributions probed here is timely. Under the present conditions the primary focus should be on the properties unique to a plume of plasma, particularly the extent to which the energy injected through IB might alter the propagation characteristics of the different plume constituents. From previous investigations on the UV PLA of several metal targets in vacuum,[16,17,24,41,42] it follows that such energy will couple more directly to motion of the primary IB absorbers, i.e., cations, than to that of the remaining electron collision partners in the plume. Such effects in turn will lead to a more pronounced increase with rising ϕ, in the terminal propagation velocities of monatomic cations than in those of nascent neutral atoms. Indeed, the present findings on the ϕ-dependences of the $\langle T \rangle$ values for the various $Ba^{z+}(z<2)$ velocity distributions follow qualitatively such trends and, particularly, those reported by Claeyssens *et al.*[24] in studying the 193 nm PLA of graphite. They found increasing ϕ from 5 to 20 J/cm^2 to lead to an increase in the mean velocities that characterize the total ion velocity distributions arising from that target, but to have little discernible effect on the mean kinetic energy (and thus mean velocity) of total neutral C atoms. Similar trends are displayed here by the weighted average temperatures (which are regarded as most appropriate signifiers of the propagation velocities) of many of the charged and neutral monatomic plume components, as the behaviors of the Ba^+/Ba^{2+} ions (monitored via corresponding Ba^*/Ba^{+*} emissions) and the ground-state Ba atoms, respectively, make evident. No discernible ϕ-dependences were actually observed in the measured metastable velocity distributions but, given that these are considered to be a convolution of neutral Ba(^3D_J) and Ba($^1D_2$) atoms both ejected from the target and originated from radiative decay of higher-lying excited states, the effect of ϕ on them cannot be readily ascertained. The dark-state population distribution of Ba atoms reported in Sec. III C will show up other differences between the ground and metastable state populating mechanisms.

The decrease in $\langle T \rangle$ with increasing ϕ for the Ba^{3+} ions (as viewed via the emission from $Ba^{2+}(5s^25p^54f[3/2]_2)$) merits further discussion. This is unlikely to arise from depletion of Ba^{3+} ions that is caused by an increasing abundance of higher charged ions in the plume since a similar behavior would have been expected for the Ba^+ and Ba^{2+} ions. Instead, it seems more plausible that the Ba^{3+} ions, being the fastest moving plume species, may be subjected to an increasingly reduced collisional coupling with rising ϕ as they expand more rapidly after the initial ablation pulse, thereby leading to a decrease in the widths, and thus in the $\langle T \rangle$ values of their velocity distributions at higher ϕ. As mentioned above, the occurrence of plasma shielding via e-i IB

TABLE III. Relative population distributions of low-lying electronic states of Ba atomic species. For each laser ablation fluence reported, the values given in the left column are relative to the number density of Ba($^1S_0$) at 10.8 J/cm^2, while values (in italics) in the right column indicate population distributions in percent at that particular laser ablation fluence.

Species	Excitation energy (eV)	Fluence (J/cm^2) 5.3		7.6		10.8	
Ba($^1S_0$)	0	$(407\pm33)\times10^{-3}$	*69.1*	$(565\pm45)\times10^{-3}$	*78.3*	1.000 ± 0.081	*89.4*
Ba($^3D_1$)	1.12	$(85\pm5)\times10^{-3}$	*14.5*	$(60\pm5)\times10^{-3}$	*8.4*	$(45\pm3)\times10^{-3}$	*4.1*
Ba($^3D_2$)	1.14	$(47\pm4)\times10^{-3}$	*8.0*	$(47\pm4)\times10^{-3}$	*6.6*	$(36\pm3)\times10^{-3}$	*3.3*
Ba($^3D_3$)	1.19	$(44\pm3)\times10^{-3}$	*7.6*	$(44\pm4)\times10^{-3}$	*6.0*	$(29\pm2)\times10^{-3}$	*2.6*
Ba(^3D_J)	1.15	$(177\pm12)\times10^{-3}$	*30.1*	$(151\pm12)\times10^{-3}$	*21.0*	$(111\pm9)\times10^{-3}$	*10.0*
Ba($^1D_2$)	1.41	$(4\pm2)\times10^{-3}$	*0.8*	$(5\pm2)\times10^{-3}$	*0.7*	$(7\pm2)\times10^{-3}$	*0.6*

should induce an opposite tendency, which may explain the observed slight decreases of the weighted average temperatures for Ba^{3+} with rising ϕ. These factors may also be responsible for the reduced, approximately twofold increase in $\langle T\rangle$ for the Ba^{2+} ions in comparison to the corresponding approximately three-/fourfold increase for the Ba^{+} ions (depending on the Ba^{*} emission probed) within the present fluence range (see Fig. 5), despite the Ba^{2+} ions are predicted[14] to experience as double rate of IB as the Ba^{+} ions.

C. Population distribution of low-lying (≤1.41 eV) electronic states of Ba atoms

A two-level rate equation treatment is appropriate to describe the whole LIF schemes that were used here.[43,44] This simplifies in the limits of low laser spectral energy densities $\rho(\lambda)$ at the wavelength λ of the relevant electronic transition, and short probe laser pulse durations τ_p that guarantee a fast probing of the relevant species with respect to their expansion time, such as were used here ($<2\times10^{-14}$ J/Hz^1.m^3 and 10 ns, respectively). Given the proportionality between the observed LIF intensity $I_{u\to l}$ and the number density of the upper level N_u associated to the excitation transition, this analysis leads to the following expression for $I_{u\to l}$ as a function of the time t_p after the beginning of the probe laser pulse, at any given ablation-probe distance l and delay Δt,[43,44]

$$I_{u\to l}(l,\Delta t,t_p)=\frac{\Omega}{4\pi}VG_{u\to l}\left\{N_l^0(l,\Delta t)\frac{g_u}{g_l}\rho(\lambda_{u\to l})\lambda_{u\to l}^3\times[1-\exp(-A_{u\to l}t_p)]\right\}A_{u\to l}\exp(-A_{u\to l}t_p), \tag{3}$$

where $\Omega/4\pi$ is the relative detection solid angle, V is the observation volume, $G_{u\to l}$ is the detection efficiency at the wavelength of the $u\to l$ line, and $N_l^0(l,\Delta t)$ is the initial number density of the corresponding lower level. g_i's are the statistical weights of both levels, $B_{u\to l}$ and $A_{u\to l}$ are the Einstein coefficients for $u\to l$ stimulated and spontaneous emission, respectively. This analysis ignores the possibility of orbital alignment in the atomic sample probed. The term in braces in Eq. (3) represents the absorption process, while the ensuing factors represent the subsequent fluorescence pathway back to the lower level. In this work, $N_l^0(l,\Delta t)$ corresponds to any of the number density LIF-TOF distributions of the dark-state Ba atoms that were reported on a relative scale in Sec. III B.

Integrating $I_{u\to l}$ upon both t_p and Δt gives

$$I_{u\to l}(l)=\int_0^\infty\int_0^\infty I_{u\to l}(l,\Delta t,t_p)dtd\Delta t=\frac{\Omega}{8\pi}VG_{u\to l}\frac{g_u}{g_l}\rho(\lambda_{u\to l})\lambda_{u\to l}^3N_l^0(l). \tag{4}$$

Equation (4) has been used to reduce all the integrated fluorescence intensities $I_{u\to l}(l)$ to relative populations of the various low-lying electronic states of Ba atoms within the plume at $l=3.3$ cm. There is to note that Eqs. (3) and (4) are valid in the limit of no radiation trapping by the ablation plume, which has been checked through preliminary measurements of the emission rate following excitation of the $6s6p\ ^1P_1\leftarrow6s^2\ ^1S_0$ transition line at 553.55 nm. Indeed this line may be expected to give the most serious radiation trapping effect owing to the short radiative lifetime[29] of the $^1P_1$ state and nearly closed transition cycle between the ground and excited states. From the recordings of the t_p-dependence of LIF signals within the range of Δt's used, an emission rate which agrees with the known value of $A_{P\to S}(1.19\times10^8\ \mathrm{s}^{-1})$ (Ref. 26) within 5% has been deduced. Thus, it can be considered that in the present conditions of moderate laser irradiances on the Ba surface, the ablation plume is optically thin at the given wavelength. For the transition lines used to probe the Ba metastable states, radiation trapping should be even less than that of the ground state as a result of correspondingly lower both oscillator strengths[26] and initial number densities (see below) for the former.

The resulting relative population distributions of low-lying (≤1.41 eV) electronic states of Ba atoms at the three ϕs used in this work are listed in Table III. The data at $\phi=7.6$ J/cm^2 have been previously reported,[7] and they incorporate a better estimation of the uncertainties in the population distribution determination, which mainly arise from measurement errors due to shot-to-shot fluctuations and the error in the estimation of the probe spectral energy density. No single temperature of a Boltzmann distribution could be found which fit the observed population distribution at any of

the ablation laser fluences studied here. A similar nonthermal behavior for the Nd atom metastable state population distribution has been reported in a recent nanosecond 532 nm PLA investigation of neodymium.[20] To explain such findings, electronic contributions were suggested to dominate the removal of material at the moderate ablation fluences (1 J/cm^2) of these experiments. The present proposal that a photothermal mechanism, i.e., explosive boiling do dominates the 1064 nm PLA of barium is still favored here: Within this picture, the plume constituents are not vaporized simultaneously all with the same temperature but the latter varies essentially (and largely) during vaporization, which likely leads to nonthermal population distributions. An additional factor could result from the above-suggested collisional and/or radiative cascades that would be responsible for the population of the observed Ba^{z+*} species and, particularly, of both Ba(^3D_J) and Ba($^1D_2$) metastable states which, having long lifetimes (60 and 0.25 s, respectively),[45] might act as reservoir states once the plasma expands into the collisionless regime. Ultimately, the population distributions observed at larger distances from the Ba target surface reflect some appropriate superposition of these two (or likely more) sources of nonthermal behavior. The present LIF-TOF measurements only probe such terminal population distributions, and thus do not allow these contributions to be distinguished.

It could be instructive to consider the extent to which the present results conflict with estimations of the relative populations distributions which are based on simple thermodynamic considerations. For example, the abundance in the nascent ablation vapor of Ba($^3D_1$), which lie 1.12 eV above the barium ground state would be ~0.3% of the Ba($^1S_0$) atoms if the barium surface temperature T_s within the laser focus is taken as 1913 K, i.e., the normal boiling point of barium.[46] This is lower than the observed Ba($^3D_1$) number densities at the present fluences (see Table III) by one order of magnitude. Within the present context, actually, the thermodynamic critical temperature T_{cr} of barium should be a more representative assumption for T_s; due to the lack of available data, a T_{cr} for barium of 5000 K, which is an average value for common metals,[47] can be assumed. While the resulting Ba($^3D_1$) to Ba($^1S_0$) population ratio of ~22% lies within the order of magnitude of the experimental values, neither the observed slightly decreasing Ba(^3D_J) distributions with increasing J nor the one order of magnitude lower Ba($^1D_2$) number densities would be reproduced in this case. Alternatively, the metastable populations might be estimated by assuming that a local thermal equilibrium at the translational temperature of the ejected particles is established owing to near-surface collisions or Coulombic forces that are operative in the early stages of the expansion, but the different $\langle T \rangle$ values for the various metastable velocity distributions found here prevent application of such approach. Clearly, thus, care must be exercised in assuming that thermal predictions are suited to account for the fraction of ground-state neutral species in ablation plumes generated under conditions leading to a plasma formation, as a significant buildup of population in low-lying metastable states may arise from the various excited state populating mechanisms which might be operative. Such considerations appear to be further supported by previous observations in the 532 nm PLA of Nd that some of the four lowest-lying (≤0.63 eV) $4f^4 6s^2\ ^5I_J$ metastable states of neutral Nd atoms are more heavily populated than predicted by a Boltzmann distribution.[20] The barium case is perhaps more significant in that it provides experimental evidence for the PLA of metals that laser-ablated excited atoms, i.e., Ba(^3D_J), with excitation energies higher than 1 eV and with electronic configurations completely different from that of the ground state, have number densities within the same order of magnitude than those of ablated ground-state atoms.

Admittedly that the relatively large Ba(^3D_J) and Ba($^1D_2$) number densities observed here may arise, at least in part, from possible differences between the angular distributions of the various dark-state Ba atom components. In the present study, the corresponding population distributions are derived from measurements of the total number densities of the respective neutral particles propagating along the normal to the target surface. For any given Ba dark species, the resulting number density will be highest as the directionality of its plume component with respect to the target surface normal is the greatest, i.e., most forward peaking. Unfortunately, the present experiments are not sensitive to the angular distribution of the plume components, preventing further exploration of this proposal.

The ϕ-dependence of the Ba(^3D_J) and Ba($^1D_2$) number densities, which display, respectively, a slight decrease and no discernible variation with increasing laser fluence, markedly differs from the ~2.5 times increase in the Ba($^1S_0$) number density that is observed here when ϕ is raised from 5.3 to 10.8 J/cm^2. Indeed, the latter is remarkably similar to the increase by ~1.5 in the total ablated monatomic Ba mass that was reported previously within the same range of ϕ (see Fig. 5 of Ref. 13). An increasing population in the ablation plume is what could be expected from any species that is mainly produced in the primary ablation process, like it is suggested here for the Ba($^1S_0$), as a higher laser fluence incident on the target surface should lead to an increasing total ablation yield to some extent. Moreover, as pointed out in Sec. III B, the ultimate characteristics (i.e., propagation velocities and number densities) of the neutral Ba($^1S_0$) component should be less influenced for the substantial laser-plume interactions (mainly by IB) that are predicted to occur within the prevailing fluence range. The case of the Ba(^3D_J) and Ba($^1D_2$) atoms seems more difficult to rationalize as both suggested routes for their formation, i.e., ejection from the target and radiative decay of higher-lying excited states might, in principle, be expected to increase their population in the plume with rising ϕ. This follows in the first route from those arguments used for the Ba($^1S_0$) case, and in the second one from the observed ϕ-dependence of the Ba* line intensities in the OES spectra. In the former, however, it is not apparent that metastable species with excitation energies ≥1.12 eV, should increase their population in the plume as a result of the photothermal mechanism to the same extent than the ground-state atoms. It is certainly possible that the Ba(^3D_J) and Ba($^1D_2$) number densities to have reached a plateau at the present laser fluences which, considering the relatively narrow ϕ range used here, could in turn appear as an unnoticeable variation or even a slight decrease in their

populations. On the other hand, the absence of any direct measurement of the second metastable population route makes any analysis on it virtually impossible. Further complications may arise from both routes being affected distinctly by any possible ϕ-dependence of their unresolved angular distributions of the Ba(^3D_J) and Ba($^1D_2$) components regarding those of Ba($^1S_0$). Thus, the combined measurements of the ϕ-dependences of the metastable velocity distributions and number densities make clear that the mechanisms leading to population of the Ba(^3D_J) and Ba($^1D_2$) species are much more complex than those of the remaining excited and ground-state atoms, and that processes other than those proposed above may be likely involved.

IV. CONCLUSIONS

Characteristics of the plumes arising from 1064 nm ns PLA of barium in vacuum at three moderate ϕs in the range of 5.3–10.8 J/cm^2 have been studied using both wavelength and time resolved OES and TOF-LIF. Both techniques consistently indicate that the ablated material is comprised of monatomic constituents while not revealing the presence of any small Ba$_n$ polyatomic species; in addition, LIF measurements provide a piece of evidence for the presence of delayed large particulates which are associated with the primary ablation process. Neutral atoms and both singly and doubly charged ions in excited states up to near the corresponding ionization limits are identified in the optical emission spectra, thus suggesting remarkable levels of ionization and excitation within the ablation plume. The population distributions of low-lying ($\leq$1.41 eV) dark-state neutral atoms which are derived from LIF revel that the metastable ^3D_J and $^1D_2$ abundances in the plume are higher than predictions based on assuming a Boltzmann distribution. The ^3D_J and $^1D_2$ populations are seen, respectively, to decrease slightly and nearly no vary with raising fluence, which contrasts with the increasing trend that is observed in the Ba($^1S_0$) population. At all fluences, the TOF distributions of the whole dark states and of various of the emitting species are bimodal and well described by MB and shifted MB velocity functions, respectively, with different $\langle T \rangle$ values for each state. The velocity distributions of all excited states are broader, and centered at higher TOFs (and thus velocities) than those of Ba($^1S_0$). The $\langle T \rangle$ values for the dark states are insensitive to the fluence, while for all emitting species marked variations of $\langle T \rangle$ with fluence are found. These observations have been rationalized in terms of material ejection from the target being dominated by a phase explosion mechanism, which is the main contributor to the majority Ba($^1S_0$) population. Free electrons along with cations can also be ejected from the target surface most likely through thermionic emission. At the prevailing irradiances, both charged species will arguably interact with the incident laser radiation by IB, leading to an increase in both translational and electronic energies as well as to further ionization of the various plume species. Energy input to the leading part of the expanding plume will likely be favored in such a heating mechanism, generating a fast tail of energetic electrons in advance of the remaining, cold electron distribution—the so-called two-electron-temperature mechanism. Such a heating mechanism ensures that the energy injected to the plume will alter the propagation velocities of the primary IB absorbers, i.e., cations, to a major extent than those of neutral atoms with increasing fluence. Electron-ion recombination occurring early in the plume expansion can lead to the generation of both neutral and ionic species in a manifold of long-lived Rydberg states, from which a radiative cascade will likely ensue.

The deduced ϕ-dependences of the Ba(^3D_J) and Ba($^1D_2$) populations and velocity distributions suggest that their populating mechanisms likely involve processes other than those two, i.e., vaporization from the target and radiative decay of higher-lying excited states, proposed on the basis of simply comparing their velocity distributions with those of the remaining excited and ground-state atoms.

Although this work has gone some way in elucidating the primary ablation mechanism, it is apparent that many questions still remain, particularly on the effect of ablation laser wavelengths other than 1064 nm on both the plume characteristics and the total ablated monatomic Ba mass as a function of the incident laser fluence. The latter would be especially interesting to contrast with the corresponding modeling by an extension of the treatment that was developed in Ref. 13. This will be the subject of a forthcoming investigation.

ACKNOWLEDGMENTS

We thank CONICET, FONCYT, and ACC of Argentina for financial support. One of us (M.R.) acknowledges a doctoral fellowship from CONICET.

[1] *Laser Ablation and Desorption*, edited by J. C. Miller and R. F. Haglund (Academic, San Diego, 1998).
[2] J. F. Ready, *Effects of High-Power Laser Radiation* (Academic, New York, 1971).
[3] P. R. Willmott and J. R. Huber, Rev. Mod. Phys. **72**, 315 (2000).
[4] M. N. R. Ashfold, F. Claeyssens, G. M. Fuge, and S. J. Henley, Chem. Soc. Rev. **33**, 23 (2004).
[5] D. Bäuerle, *Laser Processing and Chemistry* (Springer-Verlag, Berlin, 2000).
[6] T. J. Hughes and M. R. Levy, Phys. Chem. Chem. Phys. **2**, 651 (2000) and references of the senior author therein.
[7] M. Rossa, C. A. Rinaldi, and J. C. Ferrero, J. Chem. Phys. **127**, 064309 (2007).
[8] B. S. Zhao, M. Castillejo, D. S. Chung, B. Friedrich, and D. Herschbach, Rev. Sci. Instrum. **75**, 146 (2004).
[9] T. D. Bennett, C. P. Grigoropoulos, and D. J. Krajnovich, J. Appl. Phys. **77**, 849 (1995).
[10] T. D. Bennett, D. J. Krajnovich, and C. P. Grigoropoulos, Appl. Phys. Lett. **76**, 1659 (1996).
[11] J. W. Elam and D. H. Levy, J. Appl. Phys. **81**, 539 (1997).
[12] H. Nishikawa, M. Kanai, G. Szabo, and T. Kawai, Phys. Rev. B **61**, 967 (2000).
[13] I. Cabanillas-Vidosa, C. A. Rinaldi, and J. C. Ferrero, J. Appl. Phys. **102**, 013110 (2007).
[14] *Laser-Induced Plasmas and Applications*, edited by L. J. Radziemski and D. A. Cremers (Marcel Dekker, New York, 1989).
[15] D. B. Geohegan and D. N. Mashburn, Appl. Phys. Lett. **55**, 2345 (1989).
[16] R. W. Dreyfus, J. Appl. Phys. **69**, 1721 (1991).
[17] A. Vertes, R. W. Dreyfus, and D. E. Platt, IBM J. Res. Dev. **38**, 3 (1994).
[18] M. Rossa, C. A. Rinaldi, and J. C. Ferrero, J. Appl. Phys. **100**, 063305 (2006).
[19] V. I. Burimov, A. N. Zherikhin, and V. L. Popkov, Quantum Electron. **25**, 143 (1995).
[20] H. Wang, H. Ohba, M. Saeki, M. Miyabe, T. Shibata, H. Miyatake, and H. Iimura, Appl. Phys. B: Lasers Opt. **81**, 1127 (2005).

[21]B. M. Miles and W. L. Wiese, At. Data **1**, 1 (1969).
[22]P. Hellentin, Phys. Scr. **13**, 155 (1976).
[23]J. W. Cox and P. J. Dagdigian, J. Chem. Phys. **79**, 5351 (1983).
[24]F. Claeyssens, S. J. Henley, and M. N. R. Ashfold, J. Appl. Phys. **94**, 2203 (2003).
[25]F. Claeyssens, R. J. Lade, K. N. Rosser, and M. N. R. Ashfold, J. Appl. Phys. **89**, 697 (2001).
[26]L. Jahreiss and M. C. E. Huber, Phys. Rev. A **31**, 692 (1985).
[27]V. S. Burakov, N. V. Tarasenko, and N. A. Savastenko, Spectrochim. Acta, Part B **56**, 961 (2001).
[28]S. S. Harilal, B. O'Shay, M. S. Tillack, and M. V. Mathew, J. Appl. Phys. **98**, 013306 (2005).
[29]F. M. Kelly and M. S. Mathur, Can. J. Phys. **55**, 83 (1977).
[30]S. S. Chu and C. P. Grigoropoulos, ASME J. Heat Transfer **122**, 771 (2000).
[31]M. V. Mathew, S. S. Harilal, and M. S. Tillack, J. Phys. D: Appl. Phys. **40**, 447 (2007).
[32]L. Torrisi, Nucl. Instrum. Methods Phys. Res. B **183**, 271 (2001).
[33]R. S. Sage, U. B. Cappel, K. N. Rosser, M. N. R. Ashfold, and N. R. Walker, J. Appl. Phys. **103**, 093301 (2008).
[34]NIST Atomic Spectra Database, http://physics.nist.gov/asd3.
[35]C. R. Phipps and R. W. Dreyfus, in *Laser Ionization Mass Analysis*, edited by A. Vertes, R. Gijbels, and F. Adams (Wiley, New York, 1993).
[36]D. B. Geohegan, Appl. Phys. Lett. **62**, 1463 (1993).
[37]H. Dupendant, J. P. Gavigan, D. Givord, A. Lienard, J. P. Rebouillat, and Y. Souche, Appl. Surf. Sci. **43**, 369 (1989).
[38]A. Okano and K. Takayanagi, J. Appl. Phys. **86**, 3964 (1999).
[39]J. H. Yoo, S. H. Jeong, X. L. Mao, R. Greif, and R. E. Russo, Appl. Phys. Lett. **76**, 783 (2000).
[40]N. M. Bulgakova, A. V. Bulgakov, and O. F. Bobrenok, Phys. Rev. E **62**, 5624 (2000).
[41]A. Bogaerts, Z. Chen, R. Gijbels, and A. Vertes, Spectrochim. Acta, Part B **58**, 1867 (2003).
[42]A. Bogaerts and Z. Chen, Spectrochim. Acta, Part B **60**, 1280 (2005).
[43]U. Hefter and K. Bergmann, in *Atomic and Molecular Beam Methods*, edited by G. Scoles, D. Bassi, U. Buck, and D. Lainé (Oxford University Press, New York, 1988), Vol. I.
[44]M. Harnafi and B. Dubreuil, J. Appl. Phys. **69**, 7565 (1991).
[45]J. Migdalek and W. E. Baylis, Phys. Rev. A **42**, 6897 (1990).
[46]NIST Data Base, http://webbook.nist.gov.
[47]M. M. Martynyuk, Russ. J. Phys. Chem. **57**, 494 (1983).